

Protecting Distributed Blockchain with Twin-Field Quantum Key Distribution: A Quantum Resistant Approach

Xuan Li, and Ying Guo

Abstract—Quantum computing provides the feasible multi-layered security challenges to classical blockchain systems. Whereas, quantum-secured blockchains relied on quantum key distribution (QKD) to establish secure channels can address this potential threat. This paper presents a scalable quantum-resistant blockchain architecture designed to address the connectivity and distance limitations of the QKD integrated quantum networks. By leveraging the twin-field (TF) QKD protocol within a measurement-device-independent (MDI) topology, the proposed framework can optimize the infrastructure complexity from quadratic to linear scaling. This architecture effectively integrates information-theoretic security with distributed consensus mechanisms, allowing the system to overcome the fundamental rate-loss limits inherent in traditional point-to-point links. The proposed scheme offers a theoretically sound and feasible solution for deploying large-scale and long-distance consortium.

Index Terms—Twin-Field Quantum key distribution, Blockchain

I. Introduction

Blockchain technology establishes a decentralized, trustworthy distributed ledger system by integrating a peer-to-peer (P2P) network, a consensus mechanism and a robust cryptographic framework [1]. The security and integrity of this framework are fundamentally underpinned by classical cryptographic primitives. At its core, asymmetric encryption provides secure identity authentication. Each node possesses a public-private key pair; the public key serves as its network identifier. On this foundation, digital signatures guarantee the integrity and non-repudiation of transactions. A transaction is validated by a signature generated with the sender's private key, which any node can verify using the corresponding public key. These cryptographic guarantees are essential for the trusted operation of any blockchain.

However, the advent of quantum computing introduces profound, multi-layered security challenges to classical blockchain systems [2]–[4]. At the cryptographic layer, quantum computers running Shor's algorithm [5] can solve integer factorization

and discrete logarithm problems in polynomial time, effectively breaking mainstream asymmetric encryption schemes like Elliptic Curve Digital Signature Algorithm [6] (ECDSA) and the Rivest-Shamir-Adleman [7] (RSA). This directly compromises digital signatures and user authentication, which are the bedrock of transaction security. Furthermore, at the consensus layer, popular mechanisms like Proof-of-Work (PoW) are also vulnerable. For instance, in PoW-based public blockchains, a quantum adversary using Grover's algorithm [8] could achieve a quadratic speedup in hash computations. This would enable them to monopolize network hashing power and launch a 51% attack, subverting the ledger's integrity. These dual threats to both cryptography and consensus highlight the systemic vulnerability of classical blockchains and underscore the urgent need for a holistic, quantum-resistant architecture rather than piecemeal fixes [9]–[11].

To address the threats that quantum computing poses to blockchain systems [12], two primary countermeasures have been proposed. The first involves leveraging post-quantum cryptography [13] (PQC) algorithms to enhance blockchain security. These algorithms employ mathematical structures presumed resistant to quantum factorization and quantum search algorithms, aiming to strengthen the blockchain cryptographic layer against quantum attacks. However, the security of such algorithms remains incompletely validated to date [10]. Rigorous theoretical and practical testing is still under way, leaving their long-term unconditional security uncertain. Given the lack of comprehensive verification, a sole reliance on PQC may not ensure full protection against future quantum threats. The second, more fundamental approach involves integrating Quantum Key Distribution (QKD) technology [14]–[16]. In sharp contrast to PQC's reliance on computational assumptions, QKD provides information-theoretic security, which is unconditionally guaranteed by the laws of quantum physics - primarily the Heisenberg uncertainty principle and the no-cloning theorem. QKD's security is not contingent on an adversary's computational power, but rather on a

X. Li and Y. Guo are with the School of Computer Science, Beijing University of Posts and Telecommunications, Beijing 100876, China.

physical reality: any attempt to eavesdrop on the quantum channel by measuring the quantum states will inevitably introduce detectable disturbances. This allows legitimate parties to quantify the potential information leakage and establish a shared secret key that is provably secure. Consequently, integrating QKD offers a path toward building a truly future-proof security infrastructure for blockchain, immune to advances in both classical and quantum computing.

However, applying QKD to large-scale, multi-node networks such as blockchains encounters distinct practical constraints. The intrinsic point-to-point nature of conventional QKD systems diverges from the decentralized communication topology required by distributed ledgers. Establishing secure quantum channels across geographically dispersed nodes necessitates addressing several critical issues, including network scalability, efficient key routing among arbitrary nodes, the maintenance of sufficient key-generation rates to meet transaction throughput demands. Overcoming these implementation barriers is a prerequisite for realizing a practical quantum-secured blockchain.

Early explorations in constructing quantum-secured blockchains relied on the seminal BB84 protocol to establish secure channels [14], [16]. While BB84 offers theoretical Information-Theoretic Security (ITS) rooted in the no-cloning theorem, its application to distributed ledger systems faces fundamental practical limitations. First, owing to the lack of ideal single-photon sources, practical implementations utilizing weak coherent pulses are vulnerable to photon-number-splitting (PNS) attacks [17]–[21]. Second, BB84 is inherently ill-suited for scalable networks; its point-to-point architecture necessitates a quadratic increase in quantum channels ($O(N^2)$) for an N -node network. Furthermore, the secret key rate of BB84 decays exponentially with transmission distance, severely restricting both the geographical reach and the transaction throughput required by contemporary blockchain workloads [22].

In contrast, the Twin-Field Quantum Key Distribution (TF-QKD) protocol offers a solution that extends the scalability of quantum networks [23]. First, regarding security, TF-QKD adopts a measurement-device-independent [24] (MDI) architecture where single-photon interference occurs at an untrusted central relay. This design renders the system immune to all detector-side channel attacks, allowing the relay to remain untrusted without compromising key security. Second, in terms of performance, TF-QKD overcomes the fundamental linear rate-loss limit [22] (Pirandola-Laurenza-Ottaviani-Banchi bound, PLOB) inherent to point-to-point protocols. By enabling the secret key rate to scale with the square root of the channel

transmittance ($O(\sqrt{\eta})$), it supports high-rate key generation over inter-city distances. Crucially, this architecture naturally facilitates a scalable star-shaped topology. Unlike the mesh networks required by BB84, TF-QKD connects multiple users via a single central node, significantly reducing the infrastructure complexity ($O(N)$ links) and making it intrinsically suitable for large-scale, geographically distributed consortium blockchains.

Drawing upon the distinct long-distance capabilities of the TF-QKD protocol, this paper proposes a novel, quantum-secured blockchain architecture designed specifically for consortium networks. The primary contributions of this work are threefold:

First, we introduce a hybrid network architecture governed by a global witness mechanism. To reconcile the conflict between the symmetric nature of QKD keys and the non-repudiation requirements of blockchain, we propose a dual-key stratification strategy. This approach utilizes the high key-rate of TF-QKD to construct an information-theoretically secure one-time signature scheme [25]. By leveraging a vector of Wegman-Carter Message Authentication Codes [26] (MACs) and a delayed key disclosure protocol, we effectively transform symmetric verification into publicly auditable proof. Crucially, this mechanism enforces a strict separation between transaction evidence, which is rendered publicly verifiable, and consensus security, which remains permanently secret, thereby ensuring long-term ledger immutability.

Second, we propose a quantum-secured Byzantine Fault Tolerance [27], [28] (BFT) consensus protocol. Unlike traditional BFT implementations relying on computationally vulnerable digital signatures, our scheme employs ITS authentication codes derived from the QKD layer. This design enhances the integrity and resilience of the consensus process against both internal malicious nodes and external quantum adversaries. By integrating the authentication strictly within the permissioned consensus logic, we ensure the system's safety and liveness without computational hardness assumptions.

Finally, the proposed architecture addresses the challenges of scalability and practicality in wide-area networks. By adopting TF-QKD, our system overcomes the PLOB in traditional BB84-based point-to-point systems. This work provides a feasible roadmap for deploying quantum-safe distributed ledgers across inter-city distances, demonstrating a comprehensive solution for a distributed consortiums.

The remainder of this paper is organized as follows. Section II outlines the preliminaries and related work. Section III details the proposed architecture, integrating the TF-QKD network layer with the quantum-secured BFT consensus mech-

anism. The comprehensive security analysis and performance evaluation are presented in Section IV and Section V, respectively. Finally, Section VI concludes the paper.

II. Preliminaries and Related Work

A. Classical Blockchain and Quantum Threats

A blockchain functions as a decentralized, immutable ledger, structurally relying on a layered architecture comprising data, network, consensus, and application layers. The security of this ecosystem is strictly predicated on classical cryptographic primitives: asymmetric cryptography for digital signatures and cryptographic hash functions for data integrity and consensus. However, the emergence of quantum computing fundamentally challenges the computational hardness assumptions—specifically, the integer factorization and discrete logarithm problems—that underpin these primitives.

In classical architectures, user identity and transaction non-repudiation are guaranteed by digital signature schemes such as the ECDSA or RSA. The security of these schemes hinges on the computational infeasibility of deriving a private key from a public key using classical algorithms. Simultaneously, the consensus layer, predominantly Proof-of-Work (PoW), relies on the pre-image resistance of hash functions [29] (e.g., SHA-256). In PoW, miners expend computational resources to solve a probabilistic puzzle, ensuring ledger consistency through a "one-CPU-one-vote" mechanism.

The advent of quantum algorithms introduces fundamental existential threats to these cryptographic foundations, manifesting primarily through two computational vectors.

The first and most critical vector compromises the digital signature layer via Shor's algorithm. By offering an exponential speedup in solving both the Integer Factorization problem and the Elliptic Curve Discrete Logarithm Problem (ECDLP) [30], [31], Shor's algorithm renders widely used schemes such as RSA and ECDSA vulnerable. Unlike classical brute-force methods, which are computationally infeasible, a quantum adversary can derive a private key from a public key in polynomial time. Given that public keys are inherently transparent on the blockchain ledger, this vulnerability permits the unrestricted forgery of digital signatures, user impersonation, and arbitrary asset transfer. This exposure necessitates a fundamental transition from computational security assumptions to ITS standards.

Simultaneously, the consensus layer faces systemic subversion through Grover's algorithm. This algorithm yields a quadratic speedup for unstructured search problems, effectively reducing the complexity of finding a hash pre-image from $O(2^n)$

to $O(2^{n/2})$. While increasing hash length may mitigate specific collision attacks regarding data integrity, the threat to PoW consensus remains structural. Specifically, Grover's algorithm provides a quadratic speedup in nonce discovery [32]. In a hybrid scenario where a single adversary possesses quantum capabilities while others rely on classical ASICs, this adversary could gain a disproportionate hashrate advantage efficiently. While PoW algorithms could theoretically be upgraded to quantum-resistant versions, such transitions are complex and do not address the probabilistic nature of PoW finality. Compared to patching PoW, transitioning to a BFT-based consensus offers a more fundamentally robust solution for strict consistency, especially when integrated with QKD-based authentication [33]. Consequently, this work advocates for a paradigm shift toward a BFT consensus mechanism, authenticated via information-theoretically secure keys, as proposed in our architecture.

B. Quantum-Resistant Approaches and Rationale for TF-QKD

In response to these multifaceted quantum threats, two primary paradigms for quantum-resistant security have emerged: PQC and QKD. PQC aims to replace vulnerable algorithms like ECDSA with new classical algorithms whose security relies on mathematical problems presumed to be intractable even for quantum computers. However, PQC presents two significant limitations. First, its security is derived from computational complexity assumptions that remain mathematically unproven; history has shown that algorithms once thought secure can be broken by new mathematical insights [34]. Second, PQC only offers a patch for the cryptographic layer but does not fundamentally alter the security architecture. In contrast, QKD offers a path to ITS [35]. Its guarantees are rooted in the fundamental laws of quantum physics specifically the No-Cloning Theorem and the Uncertainty Principle rather than computational hardness. This enables a comprehensive security architecture that remains secure regardless of the adversary's future computational power.

In our proposed quantum-secured blockchain architecture, QKD is utilized to establish symmetric ITS keys between network nodes. These keys act as One-Time Pads (OTPs) or are used to generate unconditionally secure Message Authentication Codes for all communications. This mechanism effectively replaces vulnerable asymmetric digital signatures. While QKD requires an authenticated classical channel for initialization, this can be bootstrapped using a small pre-shared key. Crucially, adopting a QKD-based physical layer facilitates the transition

TABLE I: Comparison of Classical Blockchain Security Mechanisms against Quantum Threats and the Proposed Architecture.

Layer / Component	Classical Mechanism	Quantum Threat	Consequence	Proposed Solution
Identity & Integrity	Digital Signatures (ECDSA, RSA)	Shor's Algorithm (Integer Factorization)	Private key derivation; Forgery & Impersonation	ITS Authentication (via TF-QKD)
Consensus Mechanism	Proof-of-Work (PoW)	Grover's Algorithm (Quadratic Speedup)	Hashrate centralization; 51% Attack	Quantum-Secured BFT (Voting-based)
Security Basis	Computational Hardness Assumptions	Mathematical Vulnerability	Systemic Collapse	Physical Laws (Uncertainty Principle)

from energy-intensive and vulnerable mechanisms like PoW to quantum-safe voting protocols (such as BFT), thereby securing both the transaction and consensus layers.

Pioneering works [2]–[4] have experimentally demonstrated QKD-secured blockchains over urban fiber networks. However, these seminal systems typically rely on point-to-point protocols like BB84. A fundamental limitation of such architectures is the requirement for a direct physical quantum link between every pair of communicating nodes. In a distributed network, this necessitates a fully connected mesh topology, where the number of required optical fiber links scales quadratically ($O(N^2)$) with the number of nodes. This hardware complexity imposes severe constraints on network scalability and cost-efficiency.

To address current scalability limitations and potentially extend the geographical reach of blockchain networks, we propose a framework based on the TF-QKD protocol. This approach aims to contribute to quantum network design by mitigating several critical implementation challenges.

First, the framework ensures immunity to detector side-channel attacks through a MDI architecture. Unlike the traditional BB84 protocol, where security is often susceptible to imperfections in receiving detectors, our approach involves nodes (Alice and Bob) transmitting optical pulses to an untrusted central relay (Charlie) for interference measurement. Consequently, security relies exclusively on the correlations between the users' prepared states and the relay's public outcomes, maintaining system integrity even if the relay's detectors are imperfect or controlled by an adversary.

From a structural perspective, TF-QKD naturally facilitates a star-shaped physical topology, where multiple blockchain nodes connect to a single relay via optical fibers. This configuration significantly reduces physical link complexity from a quadratic $O(N^2)$ dependence to a linear $O(N)$

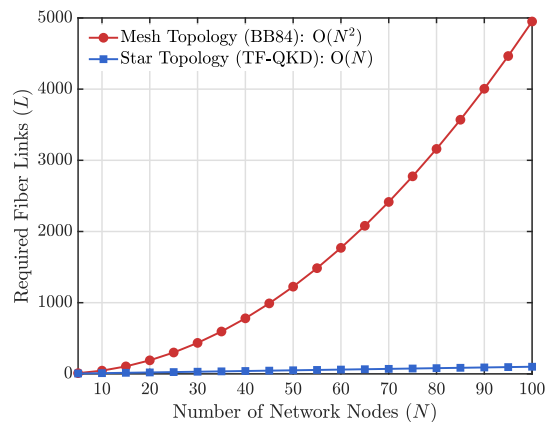


Fig. 1: Quantitative comparison of physical link complexity. The red line illustrates the quadratic growth ($O(N^2)$) of required fiber links in a traditional BB84 mesh network, utilizing the formula $L = N(N - 1)/2$. The blue line demonstrates the linear scaling ($O(N)$) of the proposed TF-QKD star topology ($L = N$). For a network of 100 nodes, the star topology reduces the link requirement by approximately 98%, significantly enhancing scalability.

scale, thereby minimizing deployment costs and simplifying network expansion. It is crucial to note that while the physical quantum layer utilizes a centralized relay, the upper-layer blockchain consensus retains its logical decentralization.

Furthermore, the protocol transcends the PLOB in point-to-point QKD. By exploiting single-photon interference, the secret key rate scales with the square root of the channel transmittance ($\sqrt{\eta}$) rather than the linear relationship (η) observed in conventional schemes. Collectively, by eliminating detector vulnerabilities, optimizing physical infrastructure, and enabling long-haul connectivity, TF-QKD provides the superior physical foundation required for practical, large-scale quantum-secured distributed ledgers.

III. Blockchain with hybrid Quantum-classical Architecture

We propose a hybrid quantum-classical architecture designed to explicitly decouple the physical key generation layer from the logical consensus layer. By implementing the TF-QKD protocol within a physical star topology, the system centralizes the complex quantum infrastructure at an untrusted relay while preserving the decentralized peer-to-peer nature of the blockchain application. This design strategy effectively translates the theoretical scalability of TF-QKD into a practical network model, ensuring a continuous and robust supply of ITS keys to support the upper layer cryptographic operations without the hardware bottlenecks of fully connected meshes.

The architecture is structured around two distinct network layers, ensuring a separation between key generation and consensus execution. The quantum layer consists of decentralized Terminal Nodes (TNs) connected via optical fibers to a central Untrusted Relay Node (URN). In this layer, the URN functions strictly as an analog interferometer, performing single-photon interference measurements required to establish pairwise ITS keys between TNs. Crucially, the URN is treated as an untrusted entity; it has no access to the generated keys, and its potential malicious behavior is limited to the interruption of key generation rather than the compromise of key confidentiality. Parallel to this, the classical layer operates as a standard P2P network (e.g., over the Internet) interconnecting all TNs. All ledger operations, including transaction broadcasting and BFT consensus voting, are conducted exclusively over this classical layer. By decoupling the consensus communication from the URN, the system ensures that the central relay does not become a bottleneck or a single point of failure for the blockchain's logical availability.

To secure the interactions within this hybrid framework, we implement a layered protocol stack. The ITS keys generated in the quantum layer are utilized to authenticate communications in the classical layer. Recognizing the high throughput requirements of blockchain systems, we adopt an authentication-based approach rather than full OTP encryption. Transaction payloads and consensus messages are transmitted in plaintext to ensure public verifiability, while their integrity and authenticity are strictly enforced via the Wegman-Carter Message Authentication Code scheme [36]. The detailed operational workflow is organized as follows: Section III-A describes the physical key establishment process and the continuous key management mechanism. Section III-B introduces the Dual-Key Stratification Strategy designed to separate transaction evidence from consensus security. Finally, the transaction lifecycle is de-

lined through Authenticated Transaction Submission (Section III-C), Decentralized Consensus (Section III-D), and Block Finalization with Key Disclosure (Section III-E).

A. Phase 1: Pairwise Key Establishment and Management

The security foundation of the proposed architecture relies on the continuous generation of ITS keys, which serve as the cryptographic anchor for authenticating classical communications. This phase is dedicated to the establishment and lifecycle management of pairwise secret keys between TNs. We adopt the TF-QKD protocol for this task. The selection of TF-QKD is motivated by two primary factors: first, its measurement-device-independent architecture effectively delegates detection processes to the URN, thereby rendering the system inherently immune to detector side-channel attacks; second, its ability to overcome the linear rate-loss limit allows for scalable key distribution suitable for the star-shaped topology of the proposed network.

The key generation process operates through a distinct separation of physical interference and classical post-processing. Functionally, for an arbitrary pair of nodes TN_i and TN_j , the process initiates with the independent preparation of phase-encoded weak coherent pulses, which are transmitted over dedicated optical fiber channels to the central URN. The URN functions solely as an interferometer, performing single-photon measurements to reveal relative phase correlations without accessing the specific encoded bit values. Following the public broadcast of measurement outcomes, TN_i and TN_j engage in a classical post-processing stage. It is important to note that this stage—comprising parameter estimation, error reconciliation, and privacy amplification—is conducted over an authenticated classical channel. This ensures that the final distilled key, K_{ij} , remains unknown to the URN.

To ensure robust system availability, key establishment is orchestrated as an asynchronous background process designed to maintain a dedicated secure key pool for each node pair. The network is bootstrapped using a small, pre-shared seed key, which establishes the initial trust basis. Subsequently, the protocol achieves self-sustainability through a dynamic replenishment mechanism, wherein a portion of the newly generated key material is reserved to authenticate future QKD post-processing messages. Furthermore, each TN implements a resource-aware scheduling strategy that actively monitors local key reserves. This mechanism prioritizes quantum transmission slots for peers whose key pools deplete below a predefined safety threshold, thereby striving to guaran-

tee that a sufficient buffer of ITS keys is available to meet the authentication demands of the consensus layer.

B. Dual-Key Stratification Strategy

To reconcile the inherent conflict between the requirement for public auditability which necessitates key disclosure and the imperative of blockchain immutability which mandates strict key secrecy we introduce a stratified key management policy. Within the proposed architecture, the TF-QKD layer is engineered to generate two distinct, ITS key streams, strictly delineated by their functional roles and lifecycle management.

The first category, designated as evidence keys (K_{evid}), is employed exclusively for the authentication of transaction payloads (M) between Terminal Nodes. These keys underpin the generation of MAC vectors and act as the foundation for the delayed key disclosure mechanism. By eventually revealing K_{evid} after block finalization, the system transforms symmetric authentication into publicly verifiable evidence, thereby ensuring non-repudiation.

In distinct contrast, the second stream comprises consensus keys (K_{cons}). These keys are strictly confined to the consensus layer, serving to authenticate Block Headers and validate voting messages during the prepare and commit phases of the BFT protocol. To preserve the structural integrity of the ledger history, K_{cons} are subject to a zero-disclosure policy; they are never revealed to the public or the untrusted relay and are securely erased immediately following the verification process.

This cryptographic bifurcation ensures that while the validity of individual transactions becomes transparent and publicly auditable post-disclosure, the blockchain's consensus history remains shielded by the undisclosed keys, rendering the chain immune to long-range forgery attacks.

C. Phase 2: Authenticated Transaction Submission via MAC Vectors

To guarantee source authenticity and non-repudiation within the broadcast network, the proposed architecture employs a vector of authenticators scheme underpinned by the evidence keys, K_{evid} . This mechanism is designed to enforce strict cryptographic synchronization across the distributed nodes while providing ITS for transaction requests. Given that the Wegman-Carter authentication scheme necessitates the strict one-time usage of secret keys, maintaining precise state synchronization between the sender and the verifiers is a prerequisite for system stability. Accordingly, each Terminal Node TN_i maintains a local, monotonically increasing transaction counter, Ctr_i .

This counter serves a dual purpose: it acts as a unique nonce to prevent replay attacks, and simultaneously functions as a deterministic pointer to the index of the QKD key within the pre-shared key pool.

When TN_i initiates a transaction with a payload M (comprising transfer details and timestamps), it constructs a global authentication vector \mathcal{V}_i to cryptographically bind the message to its origin and sequence. For a network consisting of N nodes, TN_i retrieves the specific key pair (k_{hash}, k_{otp}) corresponding to Ctr_i from the secure pool shared with each peer TN_j . The authentication tag $\tau_{i,j}$ is then computed by concatenating the counter with the message payload. This concatenation ensures that the authentication tag is inextricably linked to the specific transaction instance, thereby preventing packet reordering attacks. The mathematical formulation of the tag for each peer $j \in \{1, \dots, N\}$ is expressed as:

$$\tau_{i,j} = \begin{cases} h_{k_{hash}}(M || Ctr_i) \oplus k_{otp} & \text{if } i \neq j \\ \mathbf{0} & \text{if } i = j \end{cases}, \quad (1)$$

where $h_{k_{hash}}$ represents the universal hash function selected from the ϵ -ASU family, and $\mathbf{0}$ serves as a null placeholder for the sender's own position in the vector. The resulting authentication vector is defined as $\mathcal{V}_i = [\tau_{i,1}, \tau_{i,2}, \dots, \tau_{i,N}]$.

Following the vector construction, the transaction data is encapsulated into a formal protocol data unit, denoted as $Tx_{req} = \langle ID_i, Ctr_i, M, \mathcal{V}_i \rangle$. In contrast to centralized relay architectures, this packet is broadcast via the classical authenticated channel directly to the peer network, targeting the current consensus leader (a designated TN in the BFT protocol) rather than the central relay. It is pertinent to note that while the URN facilitates the physical generation of quantum keys in the preceding phase, it is logically excluded from this transaction submission process. The validation of the transaction format and the aggregation of Tx_{req} into a candidate block are exclusively performed by the consensus leader. By decoupling the classical transaction flow from the quantum relay, the architecture mitigates the risk of censorship or denial-of-service attacks by the URN, ensuring that the integrity of the ledger relies solely on the consensus of the TNs.

D. Phase 3: Decentralized Consensus and Verification

Upon the dissemination of the candidate block B_{cand} by the designated consensus leader (a role rotating among the TNs), the network engages in a decentralized verification protocol. To achieve robust agreement amidst potential malicious behavior, the system adapts the BFT mechanism over

the authenticated classical channel. The network model postulates n TNs accommodating at most f Byzantine adversaries, satisfying the constraint $n \geq 3f + 1$. The primary objective of this phase is to ensure that all honest nodes converge on an identical decision regarding the validity of the block proposed by the current leader, independent of the physical state of the quantum relay.

The validation process executed by each receiving node TN_j is rigorous and twofold, enforcing both cryptographic integrity and transactional semantics. First, the node verifies the authentication tags. Using the index idx_{s_j} extracted from the received vector, TN_j retrieves the corresponding one-time key pair from its local secure pool shared with the purported sender TN_s . The authentication tag is then recomputed locally for the message concatenation ($idx_{s_j} || M_k$) following the Wegman-Carter construction defined in Equation (1). A divergence between the computed and received tags, or the absence of a required authenticator, necessitates the immediate rejection of the specific transaction. Second, contingent upon successful authentication, TN_j validates the semantic legitimacy of the transaction content M_k against its local copy of the ledger state, screening for violations such as double-spending or insufficient balances. A candidate block B_{cand} is deemed valid and vote-worthy only if every constituent transaction successfully traverses this dual-verification sequence.

Following a successful validation, TN_j broadcasts its endorsement by transmitting an authenticated “ACCEPT” vote for B_{cand} directly to its peers via the classical overlay network. Finality is achieved through a quorum-based mechanism; a node considers the block irrevocably finalized once it has collected and verified a set of at least $2f + 1$ distinct and valid votes. This threshold mathematically guarantees that if any honest node commits to a block, the agreement is consistent across the honest majority, thereby preserving the safety property of the ledger.

To sustain network liveness against a faulty or malicious consensus leader such as one that ceases to propose blocks or selectively censors valid transactions the protocol incorporates a robust timeout mechanism. Should a Terminal Node fail to verify and finalize a block within a deterministic time window, a view-change protocol is triggered. In this event, the TNs utilize their secure peer-to-peer channels to establish a quorum regarding the failure of the current leader and deterministically elect a successor for the subsequent round. Crucially, since this consensus signaling occurs over the classical layer, the logical robustness of the blockchain is preserved even in scenarios where the URN encounters physical service interruptions,

provided that the local key buffers at the TNs remain sufficient to authenticate the view-change messages.

E. Phase 4: Block Finalization and Inter-Block Key Disclosure

The final phase is initiated once the consensus protocol confirms the agreement on the candidate block, denoted as B_N . Upon receiving and verifying a quorum of $2f + 1$ authenticated commit messages from the peer nodes, the terminal node promotes the candidate block to a finalized state. Subsequently, the node computes the cryptographic hash of the block header, $H(B_N)$, which incorporates the hash of the preceding block to enforce the chain-like structure. This hash value serves as a unique identifier for the block state, ensuring that the ledger history is cryptographically immutable and deterministic across all honest nodes.

While the consensus mechanism guarantees ledger consistency, the exclusive reliance on symmetric QKD keys for authentication introduces a challenge regarding public non-repudiation. To resolve this, the architecture incorporates an inter-block key disclosure mechanism, operating on a “Commit-then-Reveal” principle. Following the finalization and local storage of block B_N , the protocol mandates that every sender TN_i who successfully executed transactions within this block must disclose the specific OTP keys (part of the QKD key pairs) used to generate the authentication vectors. To optimize network bandwidth, TN_i aggregates these keys into a compact Evidence Payload. In contrast to relay-dependent approaches, this payload is broadcast directly via the classical consensus channel to the network. It is then prioritized for inclusion in the body of the subsequent block, B_{N+1} , by the elected leader of the next consensus round.

This temporal separation between key utilization and key disclosure is fundamental to the system’s security model. Since the keys for block B_N are propagated only after the block’s content has been hash-locked and immutably recorded by the honest majority, neither a malicious leader nor an external adversary can retroactively utilize the disclosed keys to forge or modify the transactions in B_N . The inclusion of the Evidence Payload in B_{N+1} effectively transforms the private, symmetric verification of the previous block into a publicly auditable record. Consequently, any network participant or external auditor can extract the keys from B_{N+1} to re-verify the MAC vectors stored in B_N . As the valid construction of a global MAC vector requires the simultaneous possession of pairwise keys shared with all nodes a condition only the legitimate sender can satisfy at the time of transmission—the successful verification of these vectors against

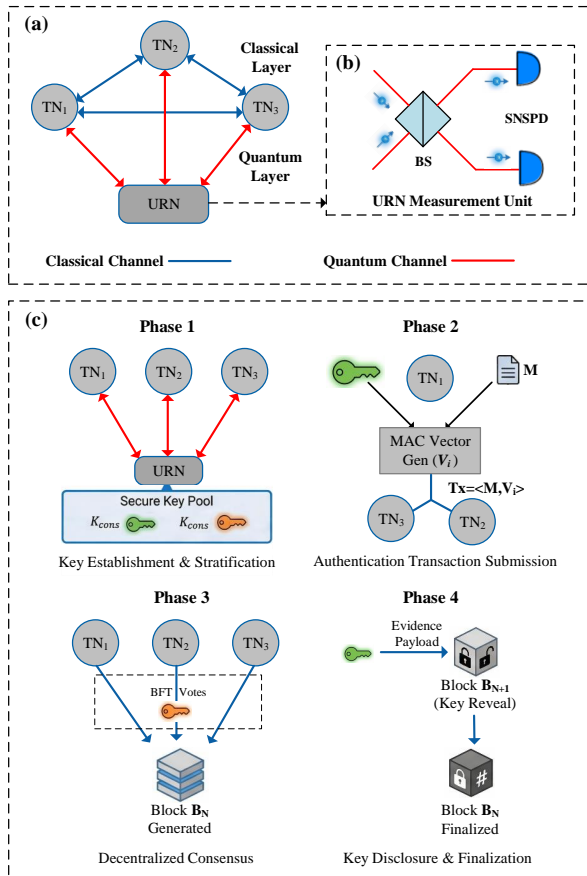


Fig. 2: Schematic overview of the proposed quantum-resistant blockchain architecture. (a) The hybrid network topology decouples the physical quantum layer from the logical classical layer. TNs connect to a central URN solely for TF-QKD interference, while consensus communications occur over a P2P classical mesh. (b) The four-phase operational workflow: Phase 1 performs continuous key stratification into Evidence Keys (K_{evid}) and Consensus Keys (K_{cons}); Phase 2 employs K_{evid} for Wegman-Carter authenticated transaction submission; Phase 3 executes decentralized BFT consensus using K_{cons} ; Phase 4 achieves block finalization and reveals K_{evid} to ensure non-repudiation.

the revealed keys provides robust cryptographic evidence of the sender’s identity.

IV. Security Analysis

In this section, we evaluate the security resilience of the proposed architecture under a comprehensive adversarial framework. Our analysis focuses on the composability of information-theoretic authentication and Byzantine Fault Tolerance consensus, demonstrating how the system mitigates threats spanning from quantum-computational attacks to internal protocol deviations.

A. Threat Model

We define a threat model that encompasses both external eavesdroppers and internal adversarial participants, operating under the assumption that the adversary possesses unbounded computational power.

External Quantum Adversary: We postulate the existence of an external adversary, Eve, equipped with unlimited computational resources, including a universal quantum computer capable of executing Shor’s and Grover’s algorithms efficiently. Under this assumption, all computational hardness primitives such as integer factorization and discrete logarithms are considered compromised. Eve is assumed to have full control over the public classical channels, granting her the capability to eavesdrop, intercept, and replay classical messages. However, her interaction with the quantum channel is strictly constrained by the fundamental laws of quantum mechanics. Specifically, the no-cloning theorem guarantees that any attempt by Eve to measure or copy the quantum states transmitted between the Terminal Nodes and the URN introduces statistically detectable disturbances, thereby preventing silent eavesdropping on the key generation process.

Internal Adversarial Participants: Regarding the network participants, we distinguish between the roles of the central relay and the decentralized terminal nodes, assigning distinct adversarial capabilities to each.

First, we model the URN as a malicious entity responsible solely for the quantum physical layer. The URN may attempt to deviate from the TF-QKD protocol by falsifying single-photon measurement results or conducting Denial-of-Service (DoS) attacks on the quantum channel to inhibit key generation. However, crucially, due to the decoupled dual-layer network architecture, the URN is assumed to have no control over the classical P2P consensus layer. Consequently, while the URN can attempt to exhaust the system’s key reservoir, it cannot suppress, modify, or censor the classical consensus messages exchanged directly between Terminal Nodes.

Second, we consider the TNs, which execute the BFT consensus protocol. We adopt the standard Byzantine failure model, assuming that an adversary may corrupt up to f nodes in a network of n participants, satisfying the condition $n \geq 3f + 1$. These Byzantine nodes may collude, behave arbitrarily, or go offline. Explicitly, this threat model includes the scenario of a malicious Consensus Leader. A compromised leader may attempt to undermine the ledger’s integrity or liveness by proposing invalid blocks, censoring specific transactions, or equivocating (broadcasting conflicting blocks to different peers). The security of the system relies

on the honest majority ($n - f$) to detect such malfeasance and trigger the view-change protocol to replace the faulty leader, ensuring the system’s resilience against authority-based attacks.

B. Immunity to Cryptographic Quantum Attacks

The central security objective of the proposed architecture is to decouple the system’s integrity from computational hardness assumptions, thereby neutralizing threats posed by known quantum algorithms. This subsection delineates the mechanisms by which the architecture addresses the specific vulnerabilities introduced by Shor’s and Grover’s algorithms.

The primary threat to transaction authenticity stems from Shor’s algorithm, which can solve the ECDLP in polynomial time, rendering conventional digital signatures (e.g., ECDSA) insecure. To circumvent this vulnerability, we substitute computational signatures with the Wegman-Carter MAC scheme. The security of this scheme is derived strictly from information-theoretic principles rather than computational complexity. Formally, for a message M , the authentication tag is computed by combining a universal hash function with a OTP:

$$Tag = H_{k_1}(M) \oplus k_2, \quad (2)$$

where H_{k_1} is selected from an ϵ -Almost Strongly Universal (ϵ -ASU) hash family using a secret key k_1 , and k_2 is a one-time encryption key. The ϵ -ASU property guarantees that the collision probability for any distinct message pair is bounded by a negligible ϵ [37]. Crucially, the subsequent XOR operation with k_2 provides perfect secrecy for the hash output. Even assuming an adversary with unbounded computational power intercepts the pair (M, Tag) , the properties of the OTP ensure that no information regarding k_1 or the tag of any subsequent message is leaked. Consequently, the probability of a successful forgery is strictly bounded by the combinatorial properties of the hash family—exponentially small relative to the tag length—rather than the adversary’s computing capabilities. A formal derivation of this bound is detailed in B.

It is imperative to note that the unconditional security of this construction is predicated on the strict "one-time" usage of the key k_2 . Key reuse would expose the system to linear cryptanalysis, where an adversary could derive the hash output via XOR linearity (e.g., $Tag_1 \oplus Tag_2 = H(M_1) \oplus H(M_2)$), potentially leading to system compromise. This constraint underscores the critical necessity of the underlying TF-QKD layer. Unlike classical systems where key distribution often forms a bottleneck, the high-rate TF-QKD protocol ensures a continuous supply of provably

secure entropy. This capability allows the system to strictly enforce a unique key policy for every transaction, thereby sustaining the theoretical security guarantees in a practical deployment.

In parallel to cryptographic integrity, the system also addresses threats to the consensus mechanism. Classical blockchains utilizing Proof-of-Work are vulnerable to Grover’s algorithm, which affords a quadratic speedup in unstructured search problems, effectively lowering the hashrate barrier for a 51% attack. The proposed architecture is intrinsically immune to this vector by adopting a voting-based BFT consensus rather than a puzzle-based mechanism. Since finality is achieved through authenticated communication quorums rather than brute-force pre-image search, there is no computational search space for a quantum adversary to accelerate. The integrity of the ledger, therefore, relies solely on the honest majority assumption ($f < n/3$) and the authentication of the voting messages, remaining robust regardless of the adversary’s quantum computational advantage.

C. Resilience to Internal Adversaries and Protocol Robustness

The system is explicitly engineered to maintain safety, liveness, and auditability despite the presence of malicious internal components. Our security analysis focuses on the distinct constraints imposed on the physical relay, the Byzantine tolerance of the consensus layer, and the cryptographic enforcement of non-repudiation.

First, regarding the URN, the proposed dual-layer architecture strictly limits its adversarial capabilities. The URN is restricted solely to the generation of raw key material. Critically, it possesses no knowledge of the distilled pairwise secret keys (K_{ij}) and is physically excluded from the classical P2P network where transaction broadcasting and consensus voting occur. Consequently, the URN is incapable of modifying transaction payloads, forging consensus votes, or censoring classical traffic. While a malicious URN may attempt a DoS attack by halting the quantum key distribution, this only impacts the replenishment of the key reservoir. The consensus protocol remains operational using buffered keys, and the system retains the capacity to trigger failover mechanisms without the URN’s participation.

Second, the system’s resilience extends to the corruption of consensus participants, including the scenario of a malicious Consensus Leader. We adopt the standard BFT assumption where the number of faulty nodes f satisfies $n \geq 3f + 1$. A compromised leader may attempt to compromise the ledger’s integrity by broadcasting invalid blocks or attempting double-spending attacks. However, the validity of any block is predicated on the

accumulation of a quorum of $2f + 1$ cryptographically authenticated votes. Since the leader cannot forge the pairwise MAC signatures of honest nodes, any attempt to fabricate a quorum or alter the immutable history will be detected by the honest majority. Furthermore, should the leader exhibit liveness failures—such as censoring valid transactions or refusing to propose blocks—the view-change protocol, executed over the authenticated P2P network, ensures that the leadership is transferred to a correct node, thereby guaranteeing continuous protocol liveness.

A critical challenge in symmetric-key systems is achieving non-repudiation without digital signatures. Our architecture addresses this through the mechanism of Information Asymmetry. Consider a scenario where a malicious receiver (e.g., Bob) attempts to frame a sender (e.g., Alice) by forging a broadcast message. In our vector-based authentication scheme, a valid broadcast requires a vector containing correct authentication tags for every node in the network. However, Bob possesses knowledge only of the specific key K_{AB} shared with Alice; he has zero knowledge of the keys Alice shares with other peers (e.g., K_{AC}, K_{AD}). Therefore, to successfully forge a global broadcast that passes verification by the network majority, Bob would need to simultaneously guess the secret keys of all other nodes, a feat that is statistically impossible absent a total collusion of the network. This asymmetry ensures that a valid MAC vector serves as undeniable proof of the sender’s origin.

Finally, to defend against Long-Range Attacks where an adversary utilizes historically disclosed keys to forge an alternative blockchain history [38] we implement a strict Dual-Key Stratification strategy. Although the Evidence Keys (K_{evid}) are eventually disclosed to facilitate public auditing, the structural integrity of the blockchain is anchored by the Consensus Keys (K_{cons}). These keys, used exclusively for authenticating block headers and linking the cryptographic chain, are never disclosed and are securely erased immediately after block finalization. This “forward secrecy” property ensures that even if an adversary gains full access to all historical transaction keys, they remain mathematically incapable of constructing valid block headers to extend a forged chain, thereby preserving the immutability of the ledger.

D. Security of the Quantum Layer

The foundational security of the proposed architecture is anchored in the information-theoretic guarantees provided by the TF-QKD protocol. Unlike classical cryptographic primitives, the security of this physical layer is derived from the fundamental postulates of quantum mechanics rather than computational complexity assumptions. In

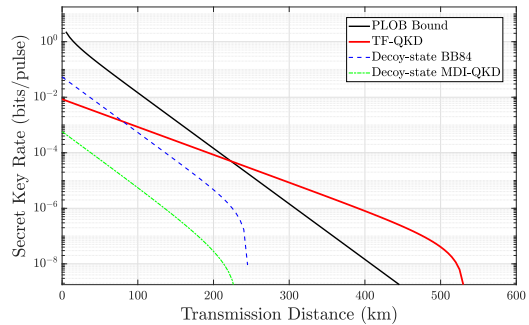


Fig. 3: Performance comparison of secret key rates. The TF-QKD protocol (red solid line) overcomes the PLOB bound (black solid line) and the distance limitations of MDI-QKD (green dash-dotted line). While BB84 (blue dashed line) shows higher rates at short distances, it lacks the measurement-device-independent security feature inherent to the TF-QKD architecture.

the implemented scheme, legitimate TNs prepare and transmit phase-encoded weak coherent pulses to the central URN. The protocol security relies on the physical reality that any eavesdropping attempt on the quantum channel inevitably disturbs the single-photon interference pattern observed at the untrusted relay. By rigorously monitoring channel parameters—specifically transmittance and phase error rates—the communicating parties can strictly bound the potential information leakage to an adversary. Through classical post-processing steps, including parameter estimation and privacy amplification, a final secret key K_{ij} is distilled. This process ensures that the adversary’s knowledge of the final key is exponentially suppressed, providing a provably secure basis for the subsequent authentication layer.

Beyond theoretical unconditionally security, the practical robustness of the physical implementation is of equal critical importance. A comparative analysis of protocol performance and security boundaries is illustrated in Fig. 3. While the traditional decoy-state BB84 protocol [39] exhibits superior key generation rates in short-to-medium haul scenarios (e.g., distances less than 200 km), its security model is predicated on the assumption of trusted measurement devices. This dependency leaves the system potentially exposed to sophisticated detector side-channel attacks, such as detector blinding or efficiency mismatch exploitation, which target imperfections in physical detection hardware.

The adoption of the TF-QKD in our system is a strategic decision to mitigate these specific physical vulnerabilities. By delegating the measurement tasks to the URN, the security proof treats the detection facility as a “black box,” thereby

removing the requirement for trusted detectors. Consequently, although TF-QKD may yield lower key rates compared to BB84 at shorter distances, it effectively eliminates the vector for detector-side channel attacks. Furthermore, regarding scalability, TF-QKD demonstrates a significant advantage in long-distance transmission. As evidenced in Fig. 3, the protocol scales with the square root of channel transmittance ($O(\sqrt{\eta})$), surpassing both BB84 and standard MDI-QKD. This characteristic allows the architecture to overcome the PLOB bound, ensuring sufficient key volume for OTP encryption even across extended metropolitan or inter-city links.

V. Performance Analysis

In this section, we establish a comprehensive analytical framework to evaluate the feasibility of the proposed quantum-secured blockchain architecture. The analysis bridges the gap between the physical layer's key generation capabilities (Supply) and the application layer's cryptographic consumption requirements (Demand).

A. Analytical Modeling Framework

To evaluate the secure key generation capacity (R_{supply}), we adopt a system level perspective. While the fundamental link physics follows the seminal TF-QKD protocol, we define R_{supply} as the aggregate secret key generation capacity of the entire network, rather than a single peer-to-peer link rate. Grounded in scalable network architectures with an adaptable star-topology, this definition highlights the use of dynamic optical switching and multi-user measurement units (MUs). This approach allows for parallel key generation among multiple user pairs, effectively bypassing the bandwidth bottlenecks associated with traditional time-division multiplexing. Consequently, our model assumes that the physical layer is capable of supporting concurrent quantum transmissions, allowing the secret key rate to scale with the square root of the channel transmittance ($O(\sqrt{\eta})$) across the network. Furthermore, to account for the impact of environmental disturbances in realistic star-topology deployments, our model incorporates the phase noise analysis framework established by Bertaina et al. [40]. The asymptotic secure key rate is derived as a function of the network radius L and the residual phase noise variance σ_ϕ . The detailed mathematical derivation, including the channel loss model, phase-matching conditions, and error rate estimation, is provided in Appendix A.

On the consumption side, the total key demand (K_{demand}) is driven by the cryptographic operations of the upper-layer blockchain protocol. The system utilizes information-theoretically

secure Message Authentication Codes (MAC) for both transaction submission and consensus voting. We introduce the following parameters to quantify this demand: the total number of terminal nodes N ; the system's target transaction throughput T (in TPS); the average number of transactions per block B ; the key length required for a single MAC authentication S_{key} ; and the average number of network-wide authentication broadcast rounds P required to complete the BFT consensus for one block.

The total key consumption is the aggregate of the bandwidth required for transaction authentication (K_{tx}) and consensus authentication (K_{con}). First, for each of the T transactions generated per second, the initiator must generate $N - 1$ independent MACs for verification by all peers. Thus, $K_{tx} = T \cdot (N - 1) \cdot S_{key}$. Second, the consensus process, operating at a rate of T/B blocks per second, requires P rounds of broadcast, where each node communicates with $N - 1$ peers. This yields $K_{con} = (T/B) \cdot P \cdot N \cdot (N - 1) \cdot S_{key}$.

Summing these components, we obtain the unified model for the system's total key consumption:

$$K_{demand}(N, T) = T(N - 1)S_{key} \left(1 + \frac{PN}{B} \right). \quad (3)$$

This equation explicitly reveals that consumption scales linearly with throughput T but quadratically ($O(N^2)$) with network size N .

It is worth noting that the proposed Dual-Key Stratification introduces a minimal overhead. Since Evidence Keys are batched and Consensus Keys are consumed per-block, the additional consumption is approximately $\Delta K \approx 1/B$. With $B = 2500$, this overhead is negligible (0.04%). Therefore, we utilize Eq. (3) as the baseline demand model.

Finally, the system's operational feasibility is governed by the supply-demand equilibrium condition:

$$R_{supply}(L, \sigma_\phi) \geq K_{demand}(N, T). \quad (4)$$

As discussed, satisfying Eq. (4) for large N relies on the aggregate capacity assumption supported by the scalable architecture. This inequality defines the feasibility boundaries evaluated in the next section.

B. Performance Evaluation and Discussion

Based on the analytical framework, we evaluate the system's performance boundaries. To ensure the results reflect a realistic high-performance deployment, we adopt the simulation parameters summarized in Table II. The physical layer parameters correspond to state-of-the-art superconducting nanowire single-photon detectors (SNSPD), while the blockchain parameters are optimized for metropolitan consortiums.

TABLE II: Simulation Parameters

Parameter	Symbol	Value
Physical Layer (TF-QKD)		
Dark Count Rate	P_d	10 Hz
Detection Efficiency	η_{det}	90%
Fiber Attenuation	α	0.2 dB/km
System Repetition Rate	f_{rep}	1 GHz
Blockchain Layer		
Block Size	B	2500 tx
Auth. Tag Length	S_{key}	64 bits
Consensus Rounds	P	3

Figure 4 illustrates the supply-demand equilibrium analysis, plotting the TF-QKD secret key generation rate (red solid line) against the key consumption requirements (dashed lines) for four distinct network scenarios ranging from minimal ($N = 4$) to medium-scale ($N = 32$) clusters. The red shaded area represents the attainable key rate envelope supported by the TF-QKD protocol. The system is operationally feasible for a given scenario only within the range where the supply curve strictly exceeds the corresponding demand threshold. The intersection points, marked as R_{max} , denote the maximum supportable network radius for each configuration.

The results demonstrate a significant trade-off between capacity and coverage. For a lightweight, wide-area scenario ($N = 4$, TPS = 10), the system supports an ultra-long coverage radius reaching approximately 165 km, validating its potential for inter-city backbone links. Intermediate configurations ($N = 8$ and $N = 16$) show a consistent decline in coverage to 111 km and 64 km respectively, following the scaling trend. Conversely, for a high-throughput metropolitan scenario ($N = 32$, TPS = 1000), the operational radius is severely constrained to approximately 14 km. This sharp reduction is attributed to the substantial surge in key consumption driven by the $O(N^2)$ growth in BFT communication overhead. This analysis confirms that the proposed architecture can flexibly adapt to diverse service requirements, effectively balancing between long-haul connectivity and high-frequency transaction processing.

To provide a holistic view of the system’s capabilities, we synthesize the constraints of network scale and coverage radius into a comprehensive feasibility map, as shown in Figure 5. This contour plot delineates the maximum achievable TPS within the parameter space of network radius (R) and node count (N). The color gradient represents the throughput magnitude on a logarithmic scale. Two key performance benchmarks are highlighted by the white contours: the solid line marks the threshold of 10^3 TPS, defining the boundary of the explicitly labeled “High-Performance Region,” while the dashed line indicates the 10^2 TPS level.

The region enclosed by the axes and the solid contour represents the optimal operating zone for commercial-grade applications. Beyond this high-performance region, the results demonstrate a flexible trade-off before reaching the “Infeasible Region” (where the system fails to sustain a secure key rate). Specifically, for a medium-scale consortium chain ($N = 50$), the architecture remains operational over a metropolitan area with a radius of up to 120 km, albeit with reduced throughput. Conversely, for extended regional links ($R \approx 180$ km), the system maintains feasibility for smaller clusters ($N \approx 10$), providing sufficient throughput for critical data logging or lightweight financial settlements. This analysis confirms that the star-topology TF-QKD architecture offers a scalable solution capable of meeting diverse application requirements within the identified feasible region.

Having established the theoretical feasibility boundaries, we extended the simulation to evaluate the system’s performance under non-ideal conditions. The analysis covers three distinct network scales: a compact metro-core ring ($R = 30$ km), a standard metropolitan coverage ($R = 50$ km), and an extended regional link ($R = 70$ km). The results regarding dynamic environmental disturbances and static hardware degradation are presented in Figure 6 and Figure 7.

We first examine the impact of dynamic phase noise σ_ϕ , which arises from environmental factors such as traffic vibrations and thermal drift. Figure 6(a) plots the transaction throughput (TPS) against the residual phase noise. The data suggests a correlation between network scale and noise tolerance. For the compact network ($R = 30$ km, blue line), the system maintains operational capability under relatively high noise conditions ($\sigma_\phi > 0.5$ rad). As the network radius expands to 50 km (red line) and 70 km (green line), the physical link loss leads to a reduction in both peak throughput and noise tolerance. All scenarios exhibit a characteristic sharp decline once the noise variance exceeds the capacity of the phase-locking feedback loop. These observations indicate that smaller network clusters may possess a larger safety margin against environmental instability.

Complementary to dynamic noise, Figure 6(b) evaluates the system’s response to static hardware degradation, modeling the cumulative effect of component aging and coupling efficiency loss (intrinsic QBER). The simulation shows a gradual decline in performance rather than an immediate failure. The multi-scale analysis indicates that shorter links appear to offer greater tolerance to hardware imperfections. For instance, while the extended 70 km link reaches its service cutoff at approximately 8.5% QBER, the 30 km link

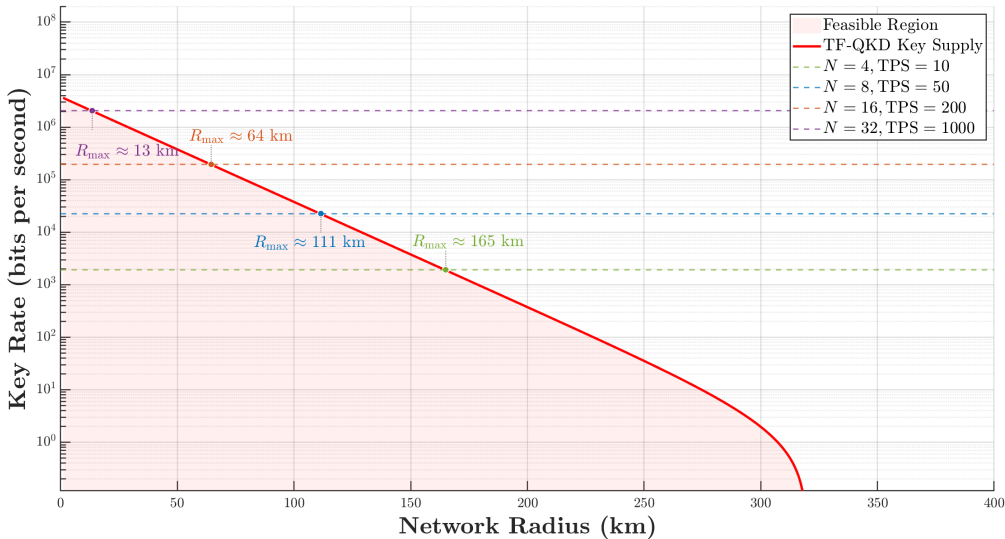


Fig. 4: Supply-demand equilibrium analysis under different network scales (N) and transaction throughputs (TPS). The red solid curve represents the TF-QKD key rate using SNSPD parameters, while the dashed lines represent the key consumption. The intersection points (R_{\max}) mark the maximum feasible network radius for each scenario.

sustains valid consensus as the intrinsic error rate approaches 9%, suggesting that lower channel loss can partially compensate for increased device noise.

Finally, to characterize the combined effect of dynamic and static disturbances, we present the joint performance landscape in Figure 7. This 3D visualization outlines the system's operational boundaries within the parameter space of phase noise and intrinsic QBER. The surface illustrates the trade-off: as environmental noise increases, the system's tolerance for hardware error decreases. This mapping provides a basis for predicting system reliability by monitoring real-time fiber noise and long-term device health.

Following the physical layer characterization, we investigated the impact of blockchain protocol configurations to identify suitable operating parameters. Focusing on a typical metropolitan scenario ($R = 50$ km, $N = 20$), the simulation results in Figure 8 quantify the throughput under varying block sizes (B) and authentication tag lengths (S_{key}). Figure 8(a) analyzes the effect of increasing block size. As B increases, the TPS shows an initial increase driven by the amortization of the consensus key consumption. However, the curve tends to saturate beyond $B \approx 2000$, where further increases yield diminishing returns while potentially introducing latency. Consequently, we consider $B \in [2000, 3000]$ as a preferred operating range. Figure 8(b) illustrates the trade-off between security and performance, showing that TPS is inversely proportional to S_{key} . While $S_{key} = 128$ bits offers higher long-term security, it reduces

throughput by approximately 50%. Given the key refreshing capabilities of QKD, $S_{key} = 64$ bits provides a calculated security margin ($\epsilon_{forge} \approx 10^{-19}$) for practical applications. Under this configuration ($R = 50$ km, $N = 20$, $B = 2500$, $S_{key} = 64$), the system achieves a peak performance of 303 TPS.

In summary, the performance evaluation supports the engineering feasibility of the proposed star-topology quantum blockchain. By integrating the physical key generation constraints of TF-QKD with the consumption dynamics of the BFT consensus, we have identified an operational region suitable for metropolitan-scale deployments. The analysis suggests that while the system is bounded by consensus communication complexity, the key rate capacity of TF-QKD appears sufficient to support reasonable throughput levels. Furthermore, the robustness simulations indicate that the architecture can tolerate a degree of environmental phase noise and hardware aging, facilitating operation under realistic deployment conditions.

VI. Conclusion

In this paper, we have proposed a quantum-resistant blockchain architecture designed to secure distributed ledgers against the computational threats posed by quantum algorithms, while addressing the scalability challenges observed in earlier QKD-integrated systems. By replacing computationally vulnerable asymmetric cryptography with information-theoretically secure Wegman-Carter authentication and substituting Proof-of-

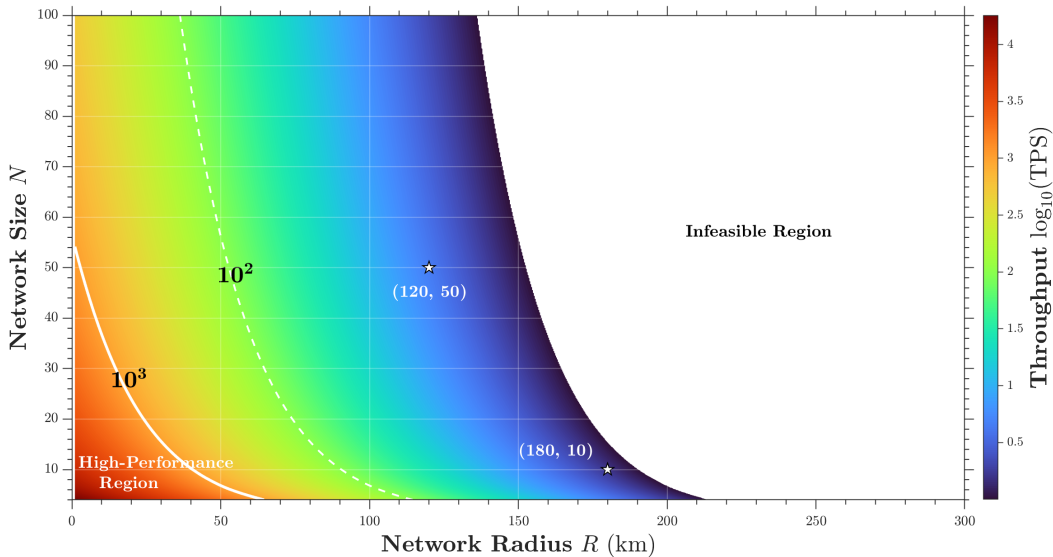


Fig. 5: Feasibility heatmap of the TF-QKD architecture showing throughput (\log_{10} TPS) as a function of network radius R and node size N . The solid white contour represents the high-performance threshold of 10^3 TPS, while the dashed contour marks 10^2 TPS. The region to the right indicates the infeasible zone where secure key generation is physically impossible. Specific operational points discussed in the text are marked: the marker at $(R = 120, N = 50)$ illustrates the limit for metropolitan consortiums, while the marker at $(R = 180, N = 10)$ demonstrates feasibility for extended regional links.

Work with a quantum-secured BFT consensus, our architecture aims to establish a security paradigm that is resilient to both Shor’s and Grover’s algorithms.

A central feature of this work is the integration of the TF-QKD protocol within a star-shaped network topology centered on an untrusted relay. This design offers a scalable alternative to traditional point-to-point BB84 schemes. Physically, the protocol overcomes the linear rate-loss limit, enabling secure key distribution over inter-city distances that are difficult to achieve without trusted repeaters. Architecturally, the star topology reduces the physical link complexity from quadratic $O(N^2)$ to linear $O(N)$, thereby lowering the infrastructure requirements for expanding consortium networks. Furthermore, the measurement-device-independent nature of TF-QKD mitigates detector side-channel risks, maintaining system security even in the presence of an untrusted central relay.

The comprehensive performance analysis, bridging physical layer constraints with consensus layer demands, supports the practical feasibility of the proposed framework. Numerical simulations indicate that the system can sustain transaction throughputs suitable for metropolitan-scale consortiums, achieving approximately 303 TPS for a network of 20 nodes with a radius of 50 km, while also supporting connectivity for longer backbone links up to 165 km. Moreover, the robustness analysis suggests that the architecture possesses

a degree of resilience against environmental phase noise and hardware degradation, indicating its potential for deployment in real-world optical fiber environments.

Future research will focus on two primary directions. First, we intend to optimize the consensus algorithm to reduce its communication complexity, thereby alleviating the key consumption overhead in larger networks. Second, we plan to explore the integration of this architecture with free-space quantum communication technologies, with the aim of extending the coverage of quantum-secured blockchains to mobile nodes and satellite-based global networks.

Appendix A

Derivation of the Asymptotic Secret Key Rate

In this appendix, we detail the theoretical framework employed to quantify the asymptotic secret key generation rate (R_{supply}) utilized in the performance analysis. To rigorously evaluate the system’s feasibility under realistic conditions, our simulation model integrates the foundational phase-matching TF-QKD protocol established by Lucamarini et al. with the environmental phase noise analysis framework derived by Bertaina et al.

We consider a standard symmetric star-topology network wherein two users, Alice and Bob, transmit optical pulses to a central Untrusted Relay Node (URN). Let L denote the total distance between the users; the fiber length from each user

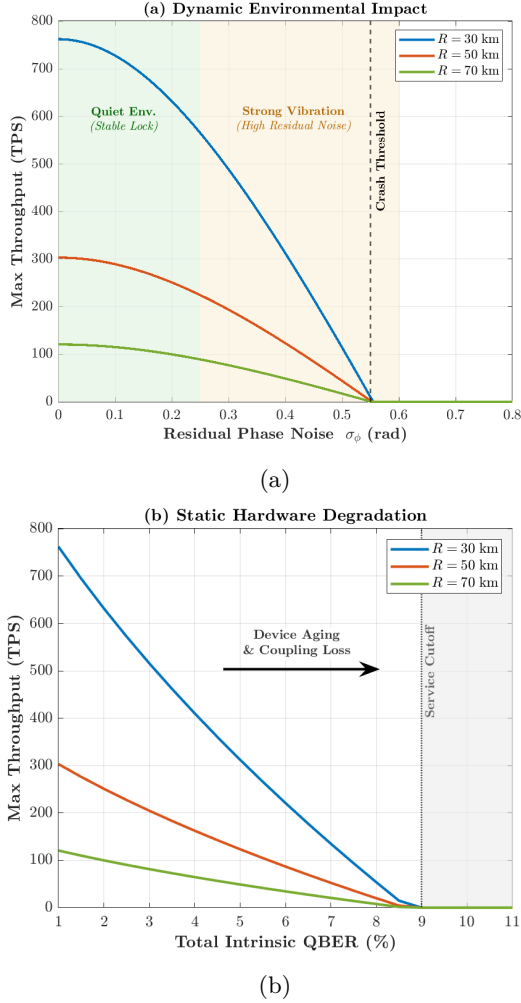


Fig. 6: Performance sensitivity analysis under individual physical constraints for varying network radius. (a) Impact of dynamic environmental phase noise (σ_ϕ) on throughput. The system exhibits a sharp cutoff behavior once noise exceeds the feedback loop’s locking range. (b) Impact of static hardware degradation (Intrinsic QBER). The results indicate that shorter links ($R = 30$ km) maintain operational consensus at higher error rates compared to extended links ($R = 70$ km), demonstrating a partial compensation effect between channel loss and device noise.

to the URN is thus $L/2$. The channel transmittance η for a single arm is modeled as:

$$\eta = \eta_{det} \cdot 10^{-\frac{\alpha L}{20}}, \quad (5)$$

where α is the fiber attenuation coefficient (typically 0.2 dB/km) and η_{det} accounts for the detection efficiency and internal optical losses.

In the phase-matching protocol, Alice and Bob encode information into phase-randomized weak coherent pulses and discretize their phase settings into M slices. The URN performs single-photon interference measurements, and valid detection

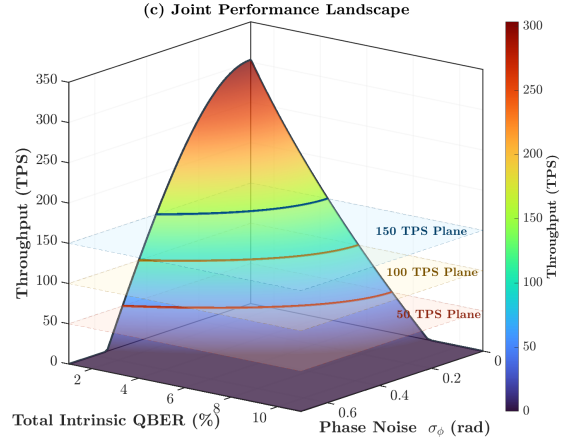


Fig. 7: Joint performance landscape illustrating the coupled impact of phase noise and intrinsic QBER on system throughput. The 3D surface represents the achievable TPS for a metropolitan network ($R = 50$ km). Horizontal semi-transparent planes are inserted at specific throughput thresholds (50, 100, and 150 TPS) to visualize service-level boundaries. The intersection contours (solid lines) define the critical trade-off frontiers: to maintain a high-performance tier (e.g., > 150 TPS, blue plane), the system requires strict control over both environmental stability ($\sigma_\phi < 0.4$) and hardware maintenance (QBER $< 4\%$).

events are retained only when the users’ phase slices match. This post-selection mechanism introduces a sifting factor of $1/M$. Furthermore, the finite discretization of the phase space introduces an intrinsic alignment error E_M , given by:

$$E_M = \frac{1}{2} - \frac{\sin(2\pi/M)}{4\pi/M}. \quad (6)$$

In our simulation, we set $M = 16$ to optimize the trade-off between the sifting efficiency and the intrinsic bit error rate.

To accurately capture the impact of environmental disturbances in field-deployed fibers—such as thermal drift and mechanical vibrations—we model the residual phase instability using the variance σ_ϕ^2 . Drawing upon the analysis in Bertaina et al., the additional error contribution induced by phase noise is approximated as $e_{noise} \approx \sigma_\phi^2/4$. This environmental error is treated as an independent noise source additive to the system’s baseline optical misalignment error, e_{opt} . Consequently, the total physical error is $e_{phy} = e_{opt} + e_{noise}$. The total phase error rate e_{ph} , governing the privacy amplification process, is derived by probabilistically combining the physical implementation error with the protocol’s intrinsic error:

$$e_{ph} = e_{phy} + E_M - e_{phy}E_M. \quad (7)$$

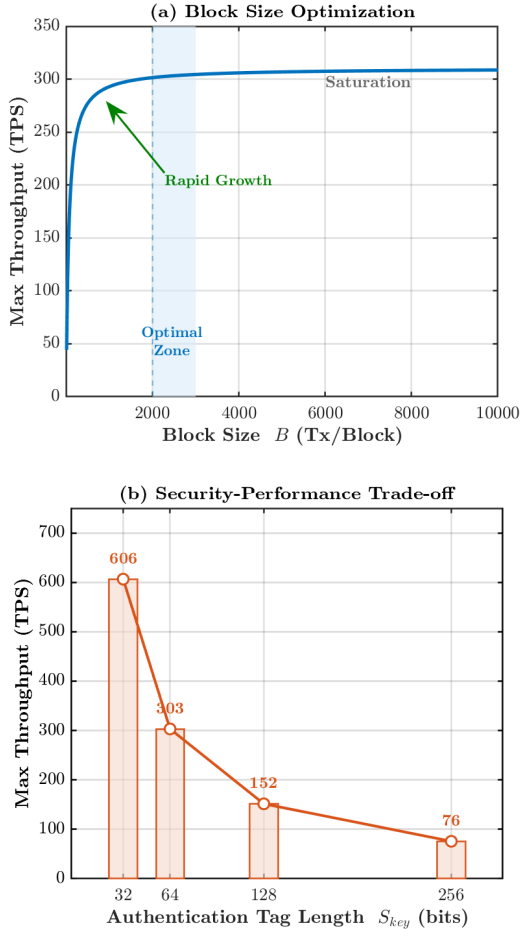


Fig. 8: Impact of blockchain protocol parameters on system performance under a metropolitan scenario (Fixed network parameters: Radius $R = 50$ km, Node count $N = 20$). (a) Throughput vs. Block Size B ($S_{key} = 64$ bits). (b) Throughput vs. Authentication Tag Length S_{key} ($B = 2500$).

This formulation allows us to evaluate the system's robustness against varying degrees of environmental noise, ranging from stable laboratory conditions to harsh field environments.

The final secure key rate is calculated using the standard decoy-state method to strictly bound the single-photon contributions. We assume the use of the vacuum+weak decoy-state method with infinite decoy intensities to simulate the asymptotic limit. Let Q_μ and E_μ represent the overall gain and quantum bit error rate for signal states with mean photon number μ , respectively. These parameters are derived from the channel transmittance and background dark count rate Y_0 . The yield of single-photon states, Y_1 , and the single-photon phase error rate are estimated based on the Poissonian photon number statistics. The asymptotic secret

key rate R is explicitly given by:

$$R = \frac{R_{rep}}{M} [\mu e^{-\mu} Y_1 (1 - H_2(e_{ph})) - f_{EC} Q_\mu H_2(E_\mu)], \quad (8)$$

where R_{rep} denotes the system repetition rate, f_{EC} is the error correction efficiency factor, and $H_2(x) = -x \log_2 x - (1-x) \log_2 (1-x)$ is the binary entropy function. This analytical model incorporates the quadratic scaling of phase noise (σ_ϕ^2) and the protocol-specific sifting penalty, providing a conservative and physically rigorous estimation of the system's performance boundaries.

Appendix B Security Bound of the Wegman-Carter Authentication

In our proposed architecture, the integrity of transactions and consensus messages is enforced via the Wegman-Carter authentication scheme. Unlike computational signatures such as ECDSA, which depend on unproven hardness assumptions, the Wegman-Carter scheme provides unconditional security resilience against quantum adversaries.

Let \mathcal{H} denote a family of ϵ -Almost XOR Universal (ϵ -AXU) hash functions mapping a message space \mathcal{M} to a tag space $\mathcal{T} = \{0, 1\}^{S_{key}}$, where S_{key} represents the bit length of the authentication tag. For an arbitrary message $m \in \mathcal{M}$, the authentication tag τ is computed as:

$$\tau = h_k(m) \oplus k_{otp}. \quad (9)$$

This construction relies on two distinct secret elements retrieved from the TF-QKD key pool: a secret hash key k , which selects a specific function $h_k \in \mathcal{H}$, and a fresh OTP key $k_{otp} \in \{0, 1\}^{S_{key}}$. A critical constraint of this protocol is that k_{otp} must be unique for every message and never reused, ensuring the scheme's information-theoretic properties.

The security of this mechanism is anchored in the perfect secrecy of the OTP. Given that k_{otp} is uniformly random and unknown to the adversary, the resulting tag τ is statistically independent of the hash output $h_k(m)$. Consequently, the observation of τ yields no information regarding $h_k(m)$ or the hash key k , regardless of the adversary's computational resources. Even a quantum adversary possessing infinite computing power cannot invert the OTP encryption to analyze the underlying hash function structure.

Under these conditions, the adversary's optimal strategy is limited to a blind forgery attempt, seeking to generate a valid tag τ' for a modified message $m' \neq m$. The probability of a successful forgery is strictly bounded by the combinatorial properties of

the ϵ -AXU hash family rather than computational hardness. This probability is derived as:

$$\begin{aligned}
 P_{forge} &= \max_{m \neq m', \tau, \tau'} \Pr_k [h_k(m') \oplus k_{otp} = \tau' \\
 &\quad | h_k(m) \oplus k_{otp} = \tau] \\
 &= \max_{m \neq m', \delta} \Pr_k [h_k(m) \oplus h_k(m') = \delta] \\
 &\leq \epsilon,
 \end{aligned} \tag{10}$$

where $\delta = \tau \oplus \tau'$ denotes the differential in the tag space.

Adopting a standard polynomial hash function over a Galois Field $GF(2^{S_{key}})$, the collision probability ϵ is determined by the ratio of the message length L to the tag space size, approximated as:

$$\epsilon \approx \frac{L}{2^{S_{key}}}. \tag{11}$$

Within the context of our simulation parameters, where $S_{key} = 64$ bits and the maximum block length is $L = 2^{20}$, the upper bound for a successful forgery is calculated as:

$$P_{forge} \leq \frac{2^{20}}{2^{64}} = 2^{-44} \approx 5.68 \times 10^{-14}. \tag{12}$$

This negligible probability confirms that the system maintains robust information-theoretic security. By consuming only 64 bits of fresh QKD key material per message, the architecture effectively eliminates vulnerabilities associated with quantum computing attacks on the authentication layer.

References

- [1] S. Nakamoto, Bitcoin: A peer-to-peer electronic cash system (2008).
- [2] A. Castiglione, J. G. Esposito, V. Loia, M. Nappi, C. Pero, M. Polsinelli, Integrating post-quantum cryptography and blockchain to secure low-cost iot devices, *IEEE Transactions on Industrial Informatics* 21 (2) (2024) 1674–1683.
- [3] A. K. Fedorov, E. O. Kiktenko, A. I. Lvovsky, Quantum computers put blockchain security at risk, *Nature* 563 (7732) (2018) 465–467.
- [4] A. Olushola, S. Meenakshi, Cybersecurity crimes in cryptocurrency exchanges (2009–2024) and emerging quantum threats: the largest unified dataset of cex and dex incidents, *Frontiers in Blockchain* 8 (2025) 1713637.
- [5] P. W. Shor, Algorithms for quantum computation: discrete logarithms and factoring, in: *Proceedings 35th annual symposium on foundations of computer science*, Ieee, p. 124–134.
- [6] D. Johnson, A. Menezes, S. Vanstone, The elliptic curve digital signature algorithm (ecdsa), *International journal of information security* 1 (1) (2001) 36–63.
- [7] R. L. Rivest, A. Shamir, L. Adleman, A method for obtaining digital signatures and public-key cryptosystems, *Communications of the ACM* 21 (2) (1978) 120–126.
- [8] L. K. Grover, A fast quantum mechanical algorithm for database search, in: *Proceedings of the twenty-eighth annual ACM symposium on Theory of computing*, p. 212–219.
- [9] Z. Yang, H. Alfauri, B. Farkiani, R. Jain, R. Di Pietro, A. Erbad, A survey and comparison of post-quantum and quantum blockchains, *IEEE Communications Surveys & Tutorials* 26 (2) (2023) 967–1002.
- [10] H. Gharavi, J. Granjal, E. Monteiro, Post-quantum blockchain security for the internet of things: Survey and research directions, *IEEE Communications Surveys & Tutorials* 26 (3) (2024) 1748–1774.
- [11] B. B. Sezer, S. Akleyek, U. Nuriyev, Pp-pqb: Privacy-preserving in post-quantum blockchain-based systems: A systematization of knowledge, *IEEE Access* (2025).
- [12] M. Wazid, A. K. Das, Y. Park, Generic quantum blockchain-envisioned security framework for iot environment: architecture, security benefits and future research, *IEEE Open Journal of the Computer Society* 5 (2024) 248–267.
- [13] M. Kumar, P. Pattnaik, Post quantum cryptography (pqc)-an overview, in: *2020 IEEE High Performance Extreme Computing Conference (HPEC)*, IEEE, p. 1–9.
- [14] E. O. Kiktenko, N. O. Pozhar, M. N. Anufriev, A. S. Trushechkin, R. R. Yunusov, Y. V. Kurochkin, A. Lvovsky, A. K. Fedorov, Quantum-secured blockchain, *Quantum Science and Technology* 3 (3) (2018) 035004.
- [15] Z. Yang, Q. Shi, T. Cheng, Q. Zhang, Q. Liu, Y. Liu, S. Peng, Qbma-biv: Quantum-key-distribution (qkd)-based multi-server authentication scheme for blockchain-enabled internet of vehicles, *IEEE Transactions on Intelligent Transportation Systems* 25 (11) (2024) 18433–18448.
- [16] N. R. Reddy, S. Suryadevara, K. G. R. Reddy, R. Umamaheswari, R. Guttula, R. Kotoju, Quantum secured blockchain framework for enhancing post quantum data security, *Scientific Reports* 15 (1) (2025) 31048.
- [17] D. Gottesman, H.-K. Lo, N. Lutkenhaus, J. Preskill, Security of quantum key distribution with imperfect devices, in: *International Symposium on Information Theory, 2004. ISIT 2004. Proceedings.*, IEEE, 2004, p. 136.
- [18] V. Scarani, H. Bechmann-Pasquinucci, N. J. Cerf, M. Dušek, N. Lütkenhaus, M. Peev, The security of practical quantum key distribution, *Reviews of modern physics* 81 (3) (2009) 1301–1350.
- [19] G. Brassard, N. Lütkenhaus, T. Mor, B. C. Sanders, Limitations on practical quantum cryptography, *Physical review letters* 85 (6) (2000) 1330.
- [20] V. Makarov, Controlling passively quenched single photon detectors by bright light, *New Journal of Physics* 11 (6) (2009) 065003.
- [21] L. Lydersen, C. Wiechers, C. Wittmann, D. Elser, J. Skaar, V. Makarov, Hacking commercial quantum cryptography systems by tailored bright illumination, *Nature photonics* 4 (10) (2010) 686–689.
- [22] S. Pirandola, R. Laurenza, C. Ottaviani, L. Banchi, Fundamental limits of repeaterless quantum communications, *Nature communications* 8 (1) (2017) 15043.
- [23] M. Lucamarini, Z. L. Yuan, J. F. Dynes, A. J. Shields, Overcoming the rate–distance limit of quantum key distribution without quantum repeaters, *Nature* 557 (7705) (2018) 400–403.
- [24] H.-K. Lo, M. Curty, B. Qi, Measurement-device-independent quantum key distribution, *Physical review letters* 108 (13) (2012) 130503.
- [25] C. E. Shannon, Communication theory of secrecy systems, *The Bell system technical journal* 28 (4) (1949) 656–715.
- [26] M. N. Wegman, J. L. Carter, New hash functions and their use in authentication and set equality, *Journal of computer and system sciences* 22 (3) (1981) 265–279.
- [27] L. Lamport, R. Shostak, M. Pease, The Byzantine generals problem, *Association for Computing Machinery (ACM)*, New York, 2019.
- [28] C.-X. Weng, R.-Q. Gao, Y. Bao, B.-H. Li, W.-B. Liu, Y.-M. Xie, Y.-S. Lu, H.-L. Yin, Z.-B. Chen, Beating the fault-tolerance bound and security loopholes for byzantine agreement with a quantum solution, *Research* 6 (2023) 0272.
- [29] D. Aggarwal, G. K. Brennen, T. Lee, M. Santha, M. Tomamichel, Quantum attacks on bitcoin, and how to protect against them, *arXiv preprint arXiv:1710.10377* (2017).
- [30] P. W. Shor, Polynomial-time algorithms for prime factorization and discrete logarithms on a quantum computer, *SIAM review* 41 (2) (1999) 303–332.
- [31] K. Kishi, J. Yamaguchi, T. Izu, N. Kunihiro, Simulation of shor algorithm for discrete logarithm problems with comprehensive pairs of modulo p and order q , *IEEE Transactions on Quantum Engineering* (2025).
- [32] A. Jain, R. Praveen, V. Musale, N. Chinthamu, Y. Kumar, B. RamaKrishna, A. Shrivastava, Quantum computing and its implications for cryptography: Assessing the security and efficiency of quantum algorithms., *Library of Progress-Library Science, Information Technology & Computer* 44 (3) (2024).
- [33] A. B. Framework, Sodsbc: A post-quantum by design asynchronous blockchain framework (2023).
- [34] W. Castryck, T. Decru, An efficient key recovery attack on sidh, in: *Annual international conference on the theory and applications of cryptographic techniques*, Springer, p. 423–447.
- [35] O. Joseph, E. Dahan, I. Aviv, I. Hadar, E. Bordo, D. Pezo, Requirements engineering for integrating quantum key distribution with blockchain systems, in: *2025 IEEE 33rd International Requirements Engineering Conference Workshops (REW)*, IEEE, 2025, pp. 375–382.
- [36] J. P. Degabriele, J. Gilcher, J. Govinden, K. G. Paterson, Sok: Efficient design and implementation of polynomial hash functions over prime fields, in: *2024 IEEE Symposium on Security and Privacy (SP)*, IEEE, 2024, pp. 3128–3146.
- [37] H. Krawczyk, Lfsr-based hashing and authentication, in: *Annual International Cryptology Conference*, Springer, 1994, pp. 129–139.
- [38] E. Deirmentzoglou, G. Papakyriakopoulos, C. Patsakis, A survey on long-range attacks for proof of stake protocols, *IEEE access* 7 (2019) 28712–28725.
- [39] H.-K. Lo, X. Ma, K. Chen, Decoy state quantum key distribution, *Physical review letters* 94 (23) (2005) 230504.

- [40] G. Bertaina, C. Clivati, S. Donadello, C. Liorni, A. Meda, S. Virzì, M. Gramegna, M. Genovese, F. Levi, D. Calonico, et al., Phase noise in real-world twin-field quantum key distribution, *Advanced Quantum Technologies* 7 (6) (2024) 2400032.